The roles of dystrophin and dystrobrevin : in synaptic signaling in drosophila

Potikanond, S.

CHAPTER 2

RhoGAP *crossveinless-c* Interacts with *Dystrophin* and is Required for Synaptic Homeostasis at the *Drosophila* Neuromuscular Junction

RhoGAP *crossveinless-c* Interacts with *Dystrophin* and is Required for Synaptic Homeostasis at the *Drosophila* Neuromuscular Junction

Gonneke S. K. Pilgram, Saranyapin Potikanond, Mariska C. van der Plas, Lee G. Fradkin, and Jasprina N. Noordermeer

Laboratory of Developmental Neurobiology, Department of Molecular and Cell Biology, Leiden University Medical Center, 2300 RC Leiden, The Netherlands

Published in The Journal of Neuroscience, 12 January 2011, 31(2): 492-500.

Abstract

Duchenne muscular dystrophy is caused by mutations in the Dystrophin gene and is characterized by muscle degeneration and the occurrence of mental deficits in a significant number of patients. Although Dystrophin and its closely related ortholog Utrophin are present at a variety of synapses, little is known about their roles in the nervous system. Previously, we reported that absence of postsynaptic Dystrophin from the *Drosophila* neuromuscular junction (NMJ) disrupts synaptic homeostasis, resulting in increased stimulus-evoked neurotransmitter release. Here, we show that RhoGAP crossveinless-c (*cv-c*), a negative regulator of Rho GTPase signaling pathways, genetically interacts with Dystrophin. Electrophysiological characterization of the *cv-c*-deficient NMJ and the use of presynaptic- and postsynaptic-specific transgenic rescue versus RNA interference reveal that the absence of postsynaptic *cv-c* results in elevated evoked neurotransmitter release. The *cv-c* mutant NMJ exhibits an increased number of presynaptic neurotransmitter release sites and higher probability of vesicle release without apparent changes in postsynaptic glutamate receptor numbers or function. Moreover, we find that decreasing expression of the Rho GTPase Cdc42 suppresses the high neurotransmitter release in the *cv-c* and Dystrophin mutants, suggesting that Cdc42 is a substrate of *cv-c*. These results indicate that Dystrophin and the Rho GTPase signaling pathway likely interact at the postsynaptic side of the NMJ to maintain synaptic homeostasis. The absence of this postsynaptic pathway results in presynaptic structural and functional alterations, suggesting that retrograde signaling mechanisms are affected. **Keywords:** *Drosophila*, synaptic homeostasis, RhoGAP, neuromuscular junction, Dystrophin, DGC

Introduction

Duchenne Muscular Dystrophy (DMD), the most common inherited muscle degenerative disease, is caused by the absence of *Dystrophin* (Hoffman et al., 1987; Koenig et al., 1987). With its interacting partners in the Dystrophin Glycoprotein Complex (DGC), Dystrophin's best studied functions are at the sarcolemma where it protects the muscle against contraction-induced injury and acts as a scaffold to localize a variety of signaling pathway components (reviewed in Rando, 2001). The observations that a significant number of DMD patients display mental deficits (Rapaport et al., 1991; Anderson et al., 2002) and that Dystrophin, its ortholog, Utrophin, and other members of the DGC are present at a variety of synapses indicate that Dystrophin also plays as yet poorly understood roles in the nervous system (reviewed in Waite et al., 2009; Pilgram et al., 2010).

The remarkable evolutionary conservation of Dystrophins' domain structure suggests that at least some of its interactions and functions are conserved. Recent studies have demonstrated the utility of the fruit fly *Drosophila melanogaster*, with its single *Dystrophin* (*Dys*) gene (Roberts and Bobrow, 1998), as a model for exploration of *Dys*'s roles at both extrasynaptic (Christoforou et al., 2007; Shcherbata et al., 2007; van der Plas et al., 2007; Kucherenko et al., 2008; Taghli-Lamallem et al., 2008) and synaptic (van der Plas et al., 2006; Fradkin et al., 2008) sites. We previously reported that the Dys DLP2 isoform is enriched at the postsynaptic side of the larval neuromuscular junction (NMJ) (van der Plas et al., 2006). Its absence from the muscle results in increased evoked neurotransmitter release by the presynaptic motoneuron. This led us to speculate that retrograde signaling from the muscle to motoneuron is altered in the *Dys* mutant. Retrograde signaling pathways influencing neurotransmitter release have also been inferred in previous murine and *Drosophila* studies (Plomp et al., 1992; Davis and Bezprozvanny, 2001; Turrigiano and Nelson, 2004), including those focused on the *Drosophila* larval NMJ (Marques and Zhang, 2006). Little is known, however, about their intra- and intercellular components.

To identify genes encoding Dys-interacting proteins, including possibly those involved in retrograde signaling, we performed a candidate-based genetic screen in the *Drosophila* wing. Here, we show that the Rho-GTPase activating protein (RhoGAP) encoding gene, *crossveinless-c* (*cv-c*) interacts with *Dys* during formation of the wing posterior crossvein. RhoGAPs counteract the Rho-GTPase exchange factors (RhoGEFs) to inhibit Rho signaling pathways in a variety of biological processes (reviewed in Hall, 1998). They increase the intrinsic GTP hydrolysis rates of Rho-GTPases leading to the accumulation of inactive GDP-bound protein.

We demonstrate in transgenic RNA interference (RNAi) and rescue studies that, as in the Dys-deficient mutant, evoked presynaptic neurotransmitter release is significantly enhanced at the NMJ when Cv-c is lacking postsynaptically. Our analyses indicate that this is likely attributable to the observed increase in neurotransmitter release sites, leading to an elevated probability of vesicle release. Heterozygosity for a null allele of the Rho GTPase Cdc42 can suppress the increased neurotransmitter release observed in *cv-c* and *Dys* mutants, supporting our hypothesis that the interaction of *Dys* with Rho signaling pathways is required for appropriate synaptic homeostasis at the NMJ.

Materials and Methods

Fly stocks

The following mutant alleles were used in the genetic enhancer screen and obtained from the Bloomington *Drosophila* Stock Center: sog^{U2}, sax^{4}, tkv^{7}, $cv\text{-}2^{1}$, wit^{B11}, wit^{A12}, $cv\text{-}d^{1}$, $egfr^{f2}$, $cv\text{-}c^{1}$, dpp^{hr92}, mys^{ts2}, $mys^{olfC\text{-}x3}$, $dNOS^{C}$, h^{1}, det^{1}, ab^{1}, ast^{1}, cg^{1}, $kni^{ri\text{-}1}$, tt^{1}, $rho^{ve\text{-}1}$, ci^{w}, ci^{1} and H^{1}. gbb^{4} and gbb^{1} were obtained from M. O'Connor. w^{1118}, the genetic background in which the *Dys* mutation was generated, served as the wild type control genotype for stainings, electrophysiology, and transmission electron microscopy analyses. The *Dys* DLP2 isoform null mutant allele, Dys^{E6}, was described previously (van der Plas et al., 2006). The *cv-c* mutant alleles $cv\text{-}c^{1}$, $cv\text{-}c^{C524}$ and UAS-*cv-c*-RNA interference flies (Billuart et al., 2001) were obtained from the Bloomington *Drosophila* Stock Center; $cv\text{-}c^{M62}$ and UAS-*cv-c*-RA (Denholm et al., 2005) were gifts from R. Ray. All *cv-c* genetic lesions are described (Denholm et al., 2005). The *cv-c* alleles were derived from distinct genetic backgrounds. To minimize possible genetic background effects, we backcrossed each allele against wild type control flies for 5 generations prior to using them in electrophysiological analyses.

The following GAL4 driver lines were used: 24B-GAL4 (Brand and Perrimon, 1993), G14-GAL4 (Aberle et al., 2002), ELAV-GAL4 (Luo et al., 1994), and OK6-GAL4 (Aberle et al., 2002). The UAS-bearing GS12472 P-element insertion (Toba et al., 1999), 1.9 kb upstream of the DLP2 ATG initiator codon, was used to express DLP2.

Genetic enhancer screen

The Dys^{E6} cross wing vein phenotype described below was used as the basis for a genetic enhancer screen. Stocks bearing mutant alleles of candidate genes (**Table 1**) previously reported to be involved in wing vein morphogenesis were crossed with Dys^{E6} at 25°C to generate trans-heterozygous progeny (e.g., Dys^{E6}*/+; mutant gene X/+* or Dys^{E6}*/mutant gene X).* Adult fly wing crossveins were scored 5 days post-eclosion.

Quantification of bouton number and muscle size

Body walls of third instar larvae were stained with anti-FasII (1D4) antibody from (Van Vactor et al., 1993). Photographs of body wall muscle number 4 in segments A2-A5 from 5 larvae (40 muscles in total) for each genotype were made and the muscle area determined using ImageJ (NIH). In addition, the numbers of boutons from at least 40 muscle number 4 fibers were manually counted in these same preparations.

Immunohistochemistry and RNA *in situ* hybridization

Third instar larvae were dissected in cold PBS and their body walls fixed in 4% formaldehyde in PBS and then incubated overnight at 4° C with mouse anti-Bruchpilot NC82 monoclonal antibody (Wagh et al., 2006) followed by application of goat anti-mouse Alexa Fluor 488 antibody (InVitrogen, Breda, The Netherlands). Body wall synapses were visualized by confocal microscopy (Leica TCS SL, Leica Microsystems, Heidelberg, Germany) and the number of NC82-positive domains at synapses on muscles 6 and 7 in 5 segments (A2-A6) were counted and total bouton area measured and analyzed using the Leica Application Suite software.

RNA *in situ* hybridizations were performed as described (Tautz and Pfeifle, 1989). The *cv-c* antisense RNA probe was generated by *in vitro* transcription of a linearized template plasmid containing sequences of the chromosome 3R *cv-c* gene (base pairs 10219833-10221479 of Genbank accession number AE014297.2).

Wing vein imaging

Whole adult flies were immersed in 100% EtOH and stored at -20ºC for 1 day. Wings were then dissected in 100% EtOH, equilibrated in 50% EtOH/ 50% Glycerol and then mounted in 50% EtOH/50% glycerol on a microscope slide. Photographs were made using a light microscope (Axio Scope, Zeiss, Germany) equipped with a digital camera (Axio Cam, Zeiss, Germany). Images representative of at least five female flies of each genotype are presented.

Transmission electron microscopy

Larval dissection, fixation, embedding, and sectioning were performed as described by (Lin and Goodman, 1994). Semi-serial sections of body walls from w^{1118}, Dys^{E6} and $cv\text{-}c^{1}$ mutants were prepared and electron micrographs were made of Type Ib boutons on muscles 6 and 7 using a transmission electron microscope (Tecnai 12 Biotwin, FEI, Eindhoven, The Netherlands).

Electrophysiology

Electrophysiological recordings were performed as described (van der Plas et al., 2006). Briefly, a microelectrode filled with 3 M KCl was inserted into muscle 6 (segments A3–A4) of dissected third-instar female larvae bathed in HL3 containing 0.6 mM Ca^{2+} unless described otherwise (Stewart et al., 1994). The intracellular measurements were recorded using a Geneclamp 500B amplifier (Axon Instruments, Union City, CA), low-pass filtered at 10 kHz, high-pass filtered at 0.5 Hz, and digitized using a Digidata 1322A and pClamp9 software (Axon Instruments). Miniature excitatory junction potentials (mEJPs) were recorded continuously for 1 min. 30 EJPs were recorded at 0.3 Hz stimulation after the appropriate axon was stimulated by a pulse generator (Master-8, AMPI, Jerusalem, Israel) via a suction electrode. Electrical input resistance of all muscle fibers recorded was above 4 MΩ. The mean mEJP amplitude and frequency were analyzed by using the peak detection feature of Mini-analysis 6.0 (Synaptosoft, Decatur, GA); all events were confirmed by eye. EJP amplitudes were analyzed using Clampfit 9.0 and amplitudes were normalized to a membrane potential of -60 mV. NMJ quantal content (QC) was calculated by dividing the mean EJP amplitude (calculated from 30 events) corrected for non-linear summation (B.A. Stewart, personal communication) by the mean mEJP amplitude (calculated from 100 events). Failure analyses were performed in HL3 with 0.15 mM Ca^{2+}. Paired-pulse facilitation was assessed at 0.6 mM and 0.25 mM Ca^{2+} using 50 ms interstimulus intervals.

Statistical analyses

One way ANOVA was performed with least significant differences (LSD) or Bonferroni for post hoc multiple comparisons (PASW statistics 17.0; SPSS, Chicago, IL) for statistical analyses. Differences were considered significant when $p<0.05$, see figure legends for details.

Results

Dystrophin interacts genetically with RhoGAP *cv-c* during wing crossvein formation in *Drosophila*.

To identify genes that interact with the *Drosophila Dys* DLP2 isoform, we performed a screen for genes that interact dominantly with a single copy of the Dys^{E6} allele during formation of the wing crossveins. The *Drosophila* wing exhibits a stereotypic pattern of five longitudinal (L1-5) and two crossveins, the anterior (acv) and the posterior crossvein (pcv). These veins lie between the dorsal and ventral wing surfaces. The pcv is usually at

least partially missing in the homozygous *Dys* mutant (**Fig. 1D**), while the pcv appears wild type in the heterozygous *Dys* mutant (**Fig. 1A**). This phenotype serves as an excellent basis for the identification of genes interacting with *Dys* since the absence of a crossvein does not affect viability and can be readily scored in the adult fly. The *Drosophila Dys* gene locus contains multiple promotors that regulate the transcription of at least 6 distinct isoforms: the three large isoforms, DLP1-3, and the smaller isoforms Dp186, Dp117 and Dp205 (reviewed in Pilgram et al., 2010). The pcv phenotype is caused by the homozygous loss of the large isoforms; the phenotype is observed in the mutant allele Dys^{E6} that lacks only these isoforms (van der Plas et al., 2006). The observation that the large isoforms are expressed in the developing wing disk (data not shown) is consistent with their roles in wing vein formation.

We selected a number of *Drosophila* mutants previously reported to display abnormal wing vein formation as candidates to test for interaction with Dys^{E6} (**Table1**). We generated flies heterozygous for the Dys^{E6} allele and one allele of the selected mutant alleles. Importantly, the pcv phenotype was not observed in individuals heterozygous for any of the candidate genes tested (not shown). Two of the 22 mutant genes display transheterozygous interactions with Dys^{E6}. One was *detached* (*det*) which subsequently was demonstrated to be an allele of *Dys* (Christoforou et al., 2007). The other was $cv\text{-}c^{1}$, a hypomorphic mutant allele of the RhoGAP *cv-c* gene (Denholm et al., 2005). Two additional alleles of *cv-c*, $cv\text{-}c^{M62}$ and $cv\text{-}c^{C524}$ were found to display similar trans-heterozygous interactions with Dys^{E6} (data not shown). While this screen was in progress, two other groups reported the identification of genes that interact with *Dys* during wing vein formation (Christoforou et al., 2007; Kucherenko et al., 2008), however, *cv-c* was not among them.

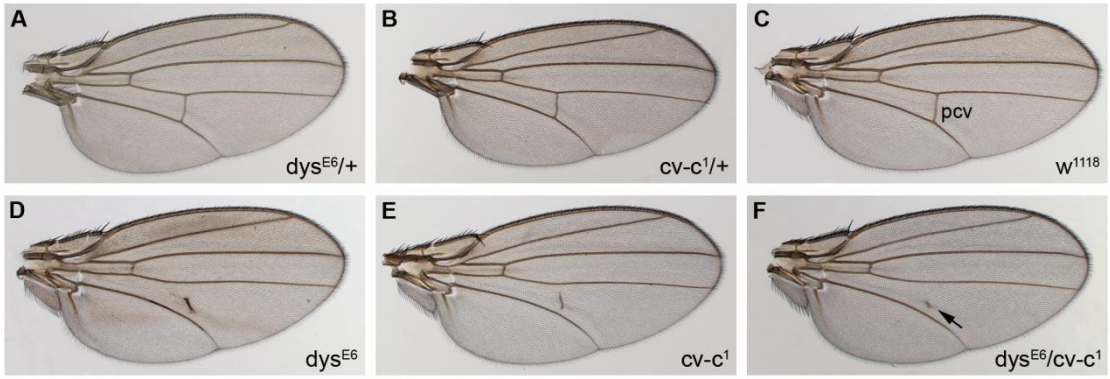

Figure 1. Dystrophin interacts genetically with *cv-c* to stabilize crossvein formation in *Drosophila* wings. Wings of heterozygous Dys^{E6}/+ (A) and $cv\text{-}c^{1}$/+ mutants (B) exhibit a wild type posterior crossvein (pcv) as in w^{1118} (C). The heterozygous double mutant $Dys^{E6}/cv\text{-}c^{1}$ (F) only has a remnant of the pcv (arrow) between the 4th and 5th longitudinal

veins left. This detached pcv phenotype is also observed in homozygous *Dys*^{E6} (D) and *cv-c*^{1} mutants (E). This result indicates a genetic interaction between *Dys* and *cv-c* in the wing.

Table 1: A candidate-based genetic screen to identify genes interacting with *Dystrophin* during wing vein formation

gene	name	alleles	function	*Dys*^{E6}/X
sog	*short gastrulation*	*sog*^{U2}	growth factor activity	-
sax	*saxophone*	*sax*^{4}	TGF-β receptor type I	-
tkv	*thickveins*	*tkv*^{7}	TGF-β receptor type I	-
gbb	*glass bottom boat*	*gbb*^{4}, *gbb*^{1}	TGF-β ligand	-
cv-2	*crossveinless-2*	*cv-2*^{1}	wing morphogenesis	-
wit	*wishful thinking*	*wit*^{B11}, *wit*^{A12}	TGF-β receptor type II	-
cv-d	*crossveinless-d*	*cv-d*^{1}	unknown	-
EGFR	*EGFR*	*egfrf*^{2}	EGFR	-
cv-c	*crossveinless-c*	*cv-c*^{1}	GTPase activator activity	+
Dpp	*decapentaplegic*	*dpp*^{hr92}	TGF-β ligand	-
mys	*myospheroid*	*mys*^{ts2}, *mys*$^{olfC-x3}$	cell adhesion molecules	-
dNOS	*Nitric oxide synthase*	*dNOS*^{C}	nitric-oxide synthase	-
h	*hairy*	*h*^{1}	tube morphogenesis	-
det	*Dystrophin*	*det*^{1}	DGC complex	+
ab	*abrupt*	*ab*^{1}	transcription factor	-
ast	*asteroid*	*ast*^{1}	muscle development	-
cg	*combgap*	*cg*^{1}	transcriptional factor	-
kni	*knirps*	*kni*$^{ri-1}$	dendrite morphogenesis	-
tt	*tilt*	*tt*^{1}	unknown	-
rho	*rhomboid*	*rho*$^{ve-1}$	serine-type peptidase	-
ci	*cubitus interruptus*	*ci*^{W}, *ci*^{1}	neuronal differentiation	-
H	*Hairless*	*H*^{1}	Notch signaling	-

The scored genetic interactions are described as: - = does not interact, + = interacts and shows altered pcv morphology. Two mutants that genetically interact with *Dys* ^{E6} in the wing were identified in this screen: *cv-c*^{1} and *det* (detached), recently identified as an allele of Dystrophin (Christoforou et al., 2008). In homozygous *cv-c*^{1}flies, 15% of wings have no pcv (crossveinless), 81% have a remnant of the pcv that does not connect with either of the two longitudinal veins (detached phenotype) and 4 % have pcv which is connected with only one of the two longitudinal veins (gap phenotype). In *Dys* ^{E6} homozygous flies, none shows a crossveinless phenotype, 81 % and 19%, display detached or gap phenotypes, respectively. No defects in pcv formation were observed in the singly heterozygous *cv-c*^{1} /+ and *Dys* ^{E6} /+ flies, while the *cv-c*^{1} / *Dys* ^{E6} transheterozygotes display no crossveinless wings, 3% and 49% detached versus gap phenotype, respectively. At least 200 wings were scored for each of the different genotypes.

RhoGAP *cv-c* regulates neurotransmitter release at the *Drosophila* larval NMJ.

Previously, we described a role for the large Dys isoform DLP2 in maintaining synaptic homeostasis at the *Drosophila* 3rd instar larval NMJ (van der Plas et al., 2006). We therefore evaluated whether *cv-c* also plays roles at this synapse. First, we determined where the *cv-c* gene is

expressed in 3rd instar larvae by RNA *in situ* hybridization (Materials and Methods). cv-c is expressed in the brain lobes but absent from the ventral nerve cord where the motoneuron cell bodies are located (**Fig. 2A**). mRNA is also present in the eye, wing and antennal imaginal disks (**Figs. 2A and 2B**), the primordia for the corresponding adult structures. Furthermore, mRNA expression is observed in the larval body wall muscle fibers (**Fig. 2C**). cv-c *m*RNA was previously found to be expressed in the embryonic visceral and somatic musculature (Denholm et al., 2005). The Dys DLP2 isoform is similarly expressed in the larval body wall musculature, eye, antennal and wing disks, and absent from the ventral nerve cord (van der Plas et al., 2006).

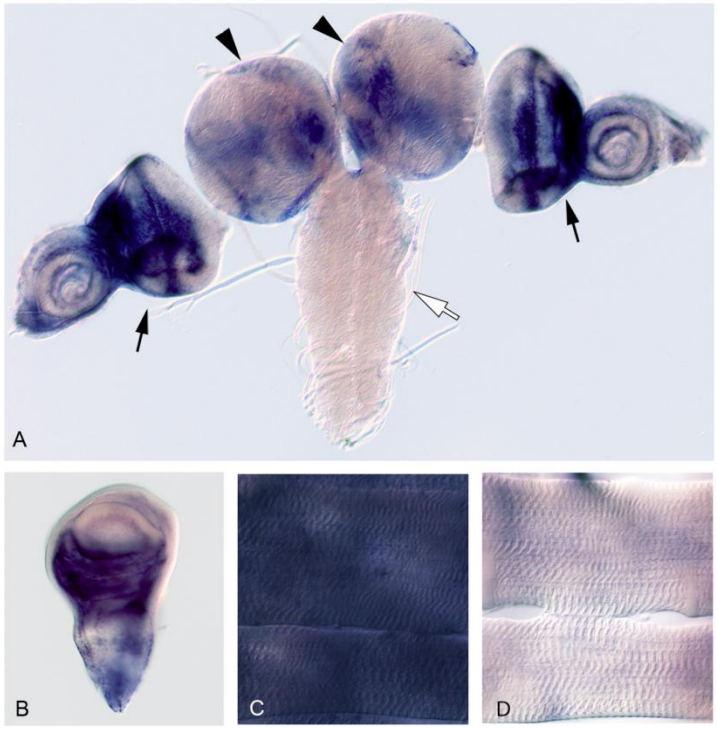

Figure 2. The RhoGAP cv-c mRNA is expressed in the third larval instar brain, wing disc and muscle fibers but not in the motoneurons. cv-c mRNA is expressed in the brain lobes (arrowheads) and the eye-antennal discs (black arrows) but not in the motoneurons and larval neuropile (white arrow) (**A**). cv-c mRNA is expressed in the wing disc (**B**) and throughout the muscle fiber (**C**). A sense strand *cv-c* probe was used as a control to determine background staining levels in muscle fibers (D).

In order to investigate the roles of Cv-c in synaptic function at the larval NMJ we performed intracellular electrophysiological recordings at an identified third instar larval muscle fiber in *cv-c* mutants and controls. We recorded three *cv-c* mutant genotypes, the hypomorphic homozygous viable $cv\text{-}c^{1}$ allele and the embryonic lethal alleles, $cv\text{-}c^{C524}$ and $cv\text{-}c^{M62}$, which were present in combination with a wild type chromosome or the $cv\text{-}c^{1}$ allele to permit collection of 3rd instar larvae. EJP amplitudes evoked by stimulation at 0.3 Hz were significantly increased above control levels, ranging from 1.4- to 1.6-fold, in all allelic combinations ($p<0.001$) (**Figs. 3A** and **3C**; measured values are given in the figure legend). Spontaneous mEJP amplitudes from the various *cv-c* mutant allelic combinations were not significantly different from control larvae (**Figs. 3A** and **3B**). QC in the *cv-c* mutant allelic combinations was, on average, approximately 70% higher than the wild type control (**Fig. 3E**). mEJP frequencies were somewhat variable between the mutants but not significantly different from wild type (**Fig. 3D**). *cv-c* is haploinsufficient for NMJ synaptic

function: the presence of one mutant allele also exhibits increased quantal content (**Fig. 3E**). Increased QC in the *cv-c* mutants was confirmed through use of an alternate method to determine neurotransmitter release levels, failure analysis (Boyd and Martin, 1956), which is independent of the mEJP amplitude. Failure analyses gave similar values to those obtained by calculating QC from the measured EJP and mEJP amplitudes (**Fig. 3F**). These results indicate that *cv-c* is required at the larval NMJ to maintain normal levels of neurotransmitter release.

We determined whether an increase in the probability of vesicle release underlies the increased QC at the *cv-c*^{1} mutant NMJ by performing paired-pulse facilitation (PPF). PPF is a form of short-term adaptation of synaptic transmission (Zucker and Regehr, 2002) and is quantified by calculation of the ratio of the amplitudes of two consecutive EJPs evoked at short interstimuli intervals. When the probability of release of EJP1 decreases, as is observed at lower external Ca^{2+} concentrations, PPF increases (Rohrbough et al., 1999; Sandstrom, 2004). Indeed, facilitation in wild type control larvae is higher (approximately 180%) at 0.25 mM external Ca^{2+} than at a Ca^{2+} concentration of 0.6 mM (approximately 115%) (**Fig. 3G**). In contrast, virtually no facilitation was observed at the *cv-c*^{1} mutant NMJ. Instead, a depression occurs at both Ca^{2+} concentrations, as though transmission during the initial EJP is already in a facilitated state (**Fig. 3G**). Therefore, we conclude that the probability of synaptic release is significantly increased at the *cv-c* mutant NMJ.

We then investigated whether the increased neurotransmitter release in the mutants was dependent on Ca^{2+} levels by comparing the QC of the mutants with the controls at different external Ca^{2+} concentrations ranging from 0.15 to 0.6 mM. The mutant QC was significantly higher than the control QC at all concentrations tested, while the slopes of the regression lines did not differ (**Fig. 3H**). These results indicate that the Ca^{2+} cooperativity is not altered in the mutant animals. Therefore, the basic properties of the Ca^{2+}-sensors that regulate Ca^{2+}-dependent vesicle fusion are not likely to be altered when RhoGAP *cv-c* levels are reduced.

RhoGAP *cv-c* is required at the postsynaptic side of the NMJ to modulate presynaptic neurotransmitter release.

We employed two different strategies to determine whether *cv-c* acts pre- or postsynaptically at the NMJ. First, we used transgenic RNA interference to reduce *cv-c* expression levels at individual sides of the synapse. Secondly, we investigated whether QC could be restored to wild type levels in the *cv-c* mutant background by expressing *cv-c* pre- versus postsynaptically. We used the UAS-GAL4 transcriptional activation system (Brand and Perrimon, 1993) to effect tissue specific expression of either double stranded (ds) RNA (Billuart et al., 2001) or a *cv-c* cDNA (Denholm et al., 2005). The G14-GAL4 and OK6-GAL4 drivers (Aberle et al., 2002) were used for pan-muscle and pan-motoneuron expression, respectively.

Expression of *cv-c* dsRNA in the motoneuron (OK6/RNAi-*cv-c)* increased QC somewhat, however the increase was not significant when compared to OK6-GAL4 driver only control (**Fig. 4**). In contrast, reduction of *cv-c* expression in the muscle (G14/RNAi-*cv-c*) resulted in significantly increased QC, phenocopying the *cv-c* mutant phenotype. Moreover, rescue of the *cv-c*^{1} phenotype was only observed when *cv-c* expression was restored in the muscle in the heterozygous mutant background (QC=47.9 ± 7.1 in G14/+;*cvc*^{1}/UAS-*cv-c*-RA larvae; QC=62.9 ± 3.5 in G14/+;*cvc*^{1}/+ control larvae) and not in the motoneuron (QC=65.2 ± 8.8 in OK6/+;*cv-c*^{1}/UAS- *cv-c*-RA larvae). These results indicate that *cv-c* acts postsynaptically to maintain wild type levels of neurotransmitter

release at the NMJ, a finding that is consistent with our observations that *cv-c* is expressed in muscle but not detected in motoneuron cell bodies.

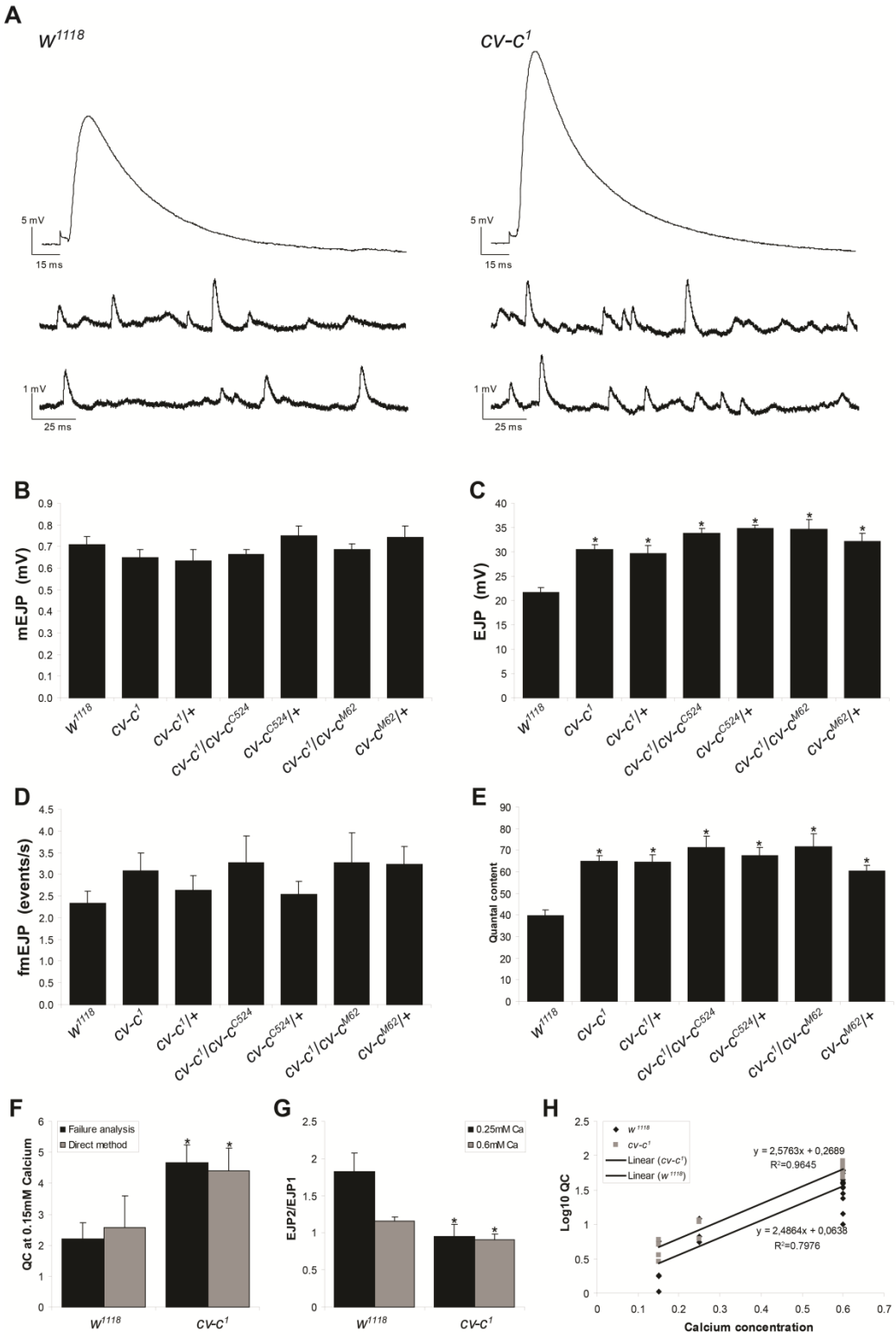

Figure 3. Electrophysiological recordings reveal that *cv-c* mutants have a Ca^{2+} independent increased QC compared to wild type controls. (**A**) Representative traces of EJPs and mEJPs recorded from w^{1118} controls and *cv-c*^{1} mutants. (**B-E)** Bar graph representations of mean ± SEM values of mEJP amplitudes (**B**), EJP amplitudes (**C**), mEJP frequencies (**D**), and QC (**E**) for the following genotypes: w^{1118} (n=24), *cv-c*^{1} (n=20), *cv-c*^{1}/+ (n=9), *cv-c*^{1}/*cv-c*^{C524} (n=6), *cv-c*^{C524}/+ (n=6), *cv-c*^{1}/*cv-c*^{M62} (n=6), and *cv-c*^{M62}/+ (n=7). While the mEJPs and their frequencies are not significantly different among these genotypes, the EJPs and QC of all *cv-c* mutant alleles are significantly increased compared to wild type animals. All raw data are summarized in supplemental Table 1. (**F**) Using failure analyses, the increased QC in *cv-c*^{1} mutants compared to that in w^{1118} control larvae was confirmed [QCs for w^{1118} controls versus *cv-c*^{1}, failure analysis, 2.2±0.5 versus 4.7±0.6; direct method, 2.6±1.0 versus 4.4±0.7]. (**G**) Paired-pulse facilitation is presented in the graph by the ratio of EJP2/EJP1 with an interstimulus interval of 50 ms measured at 0.25 and 0.6 mM Ca^{2+}. While facilitation occurs at both Ca^{2+} concentrations in wild type larvae (n=3 and n=6, respectively), it is absent in *cv-c*^{1} mutants (n=3 and n=12), indicating an increase in probability of release of synaptic vesicles in the latter. *p<0.05. (**H**) Graph of the QC, depicted as log10 QC, as a function of the external Ca^{2+} concentration showing that the elevated QC in *cv-c*^{1} mutants compared to wild type controls is Ca^{2+}-independent.

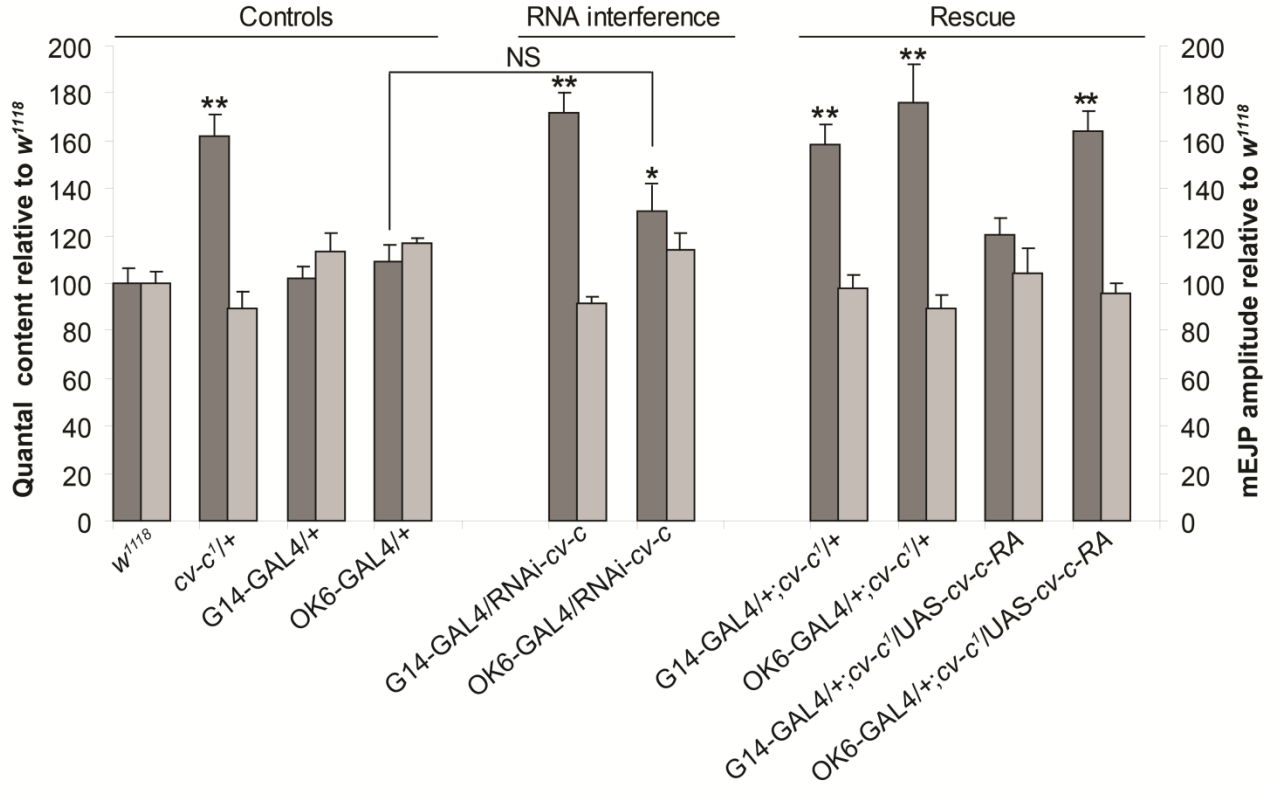

Figure 4. RNA-interference and rescue experiments reveal that RhoGAP *cv-c* is required postsynaptically at the larval NMJ. Bar graph representations are shown of the mean ± SEM values of the QC (left Y-axis, dark bars) and the mEJP amplitudes (right Y-axis, light bars) normalized to wild type controls recorded from w^{1118} third instar larvae (n=24), *cv-c*^{1}/+ (n=9), G14-GAL4/+ (n=5), OK6-GAL4/+ (n=15), G14-GAL4/RNAi-*cv-c* (n=7), OK6-GAL4/RNAi-*cv-c* (n=10), G14-GAL4/+;*cv-c*^{1}/+ (n=6), OK6-GAL4/+;*cv-c*^{1}/+ (n=6), G14-GAL4/+;*cv-c*^{1}/UAS-*cv-c*-RA (n=6), OK6-GAL4/+;*cv-c*^{1}/UAS-*cv-c*-RA (n=6). Downregulation of *cv-c* levels in muscle phenocopies the heterozygous *cv-c*^{1} elevated QC mutant phenotype, i.e. QC is 72.0% higher than w^{1118} controls. Presynaptic downregulation of *cv-c* in motoneurons results in a mild increase of about 37.0% relative to w^{1118} controls, however, this increase is not significant (NS) from its OK6-GAL4/+ driver control. Postsynaptic expression of *cv-c* in a heterozygous *cv-c*^{1} mutant background reduces the QC to wild type levels in contrast to presynaptic expression. All raw data are summarized in supplemental Table 1. Asterisks mark significant differences relative to w^{1118} controls, *p<0.05, **p<0.001.

The number of presynaptic neurotransmitter release sites is increased in the *cv-c* mutant.

The increased neurotransmitter release observed in *cv-c* mutants might be caused by changes in either the pre- or postsynaptic apparatus, such as an increases in a) presynaptic motoneuron terminal size or bouton numbers, b) the number of active zones with T-bars which are presumptive presynaptic neurotransmitter release sites or an increase in c) the number or the sensitivity of the postsynaptic neurotransmitter receptors. The *Drosophila* NMJ is a glutamatergic synapse and the best characterized postsynaptic neurotransmitter receptors subunits are GluRIIA and GluRIIB (Schuster et al., 1991; Petersen et al., 1997; DiAntonio et al., 1999; Sigrist et al., 2002; Featherstone et al., 2005). We therefore investigated whether there were apparent differences in the glutamate receptor field in the *cv-c*^{1} mutants relative to controls. No changes in the numbers and intensities of the glutamate receptor subunits GluRIIA and GluRIIB positive domains were observed (data not shown). This observation is consistent with the mEJPs recordings, mentioned above, which indicated that postsynaptic sensitivity to glutamate is unchanged in the mutant. We also counted the number of boutons and measured muscle size in *cv-c*^{1} mutants, but did not observe any differences from controls (**Suppl. Fig. 1**).

Overall *cv-c*^{1} mutant NMJ ultrastructure appeared wild type (**Fig. 5**). However, we observed an increase in the number of T-bars at the mutant NMJ relative to controls (**Fig. 5A versus 5C**). Increased numbers of T-bars were also observed at the *Dys*^{E6} mutant NMJ (**Fig. 5B**; (van der Plas et al., 2006)). We performed immunohistochemistry using an antibody that recognizes the Bruchpilot (Brp) protein which is associated with T-bar structures to quantify these apparent increases in T-bar number (**Figs. 5D-5F**; Materials and Methods) (Kittel et al., 2006; Wagh et al., 2006). We found that there is a statistically-significant 1.23-fold increase in the number of Brp^{+} zones in *cv-c*^{1} and *Dys*^{E6} boutons relative to the control (**Fig. 5G**). Thus, increased numbers of vesicle release sites in the *cv-c* mutant likely account for the higher QC observed.

Dystrophin and *cv-c* likely act in the same or parallel pathways at the NMJ.

Thus far, we have shown a genetic interaction of *cv-c*^{1} and *Dys*^{E6} during the formation of the pcv and found that these genes display similar 3rd larval instar mutant NMJ phenotypes with respect to increased levels of neurotransmitter release and increased numbers of presynaptic neurotransmitter release sites. Both genes are expressed in muscle and not apparently in the motoneuron and are required at the postsynaptic side of the synapse. Next, we set out to investigate whether the two genes interact at the NMJ. However, in contrast to their roles in wing vein formation, *Dys* and *cv-c* are haplo-insufficient for their roles in regulating neurotransmitter release (Fig. 3 and Suppl. Fig 2; van der Plas et al., 2006), preventing us from performing epistatic analyses of their function in that tissue. Moreover, the single heterozygous alleles show a similar increase in QC as observed at the transheterozygous *cv-c*1/*Dys*^{E6} NMJ, possibly indicating that the maximum level of QC is already reached in the single heterozygous alleles (Suppl. Fig 2). Therefore, we used three alternative approaches to determine whether *cv-c* and *Dys* genetically interact at the NMJ. Firstly, we investigated whether Dys expression is altered at the *cv-c*1 mutant NMJ but did not observe changes in the levels or the localization of the Dys protein (data not shown), as compared to the wild type controls. Secondly, we attempted to restore wild type neurotransmitter levels in the *cv-c*1 mutant by increasing expression levels of DLP2 in muscle or, conversely, by increasing expression levels of *cv-c* postsynaptically at the *Dys*^{E6} mutant NMJ. We used a UAS-binding site containing P-element, GS12472, inserted upstream of DLP2 (Toba et al., 1999; van de Plas et al., 2006) and a UAS-*cv-c*-

RA line (Denholm et al., 2005) driven by G14-GAL4 to increase expression of DLP2 and Cv-c, respectively, in the muscle. We observed significantly reduced QC values when DLP2 was expressed in the *cv-c*1 background, but not when Cv-c was expressed in the Dys^{E6} mutant background (Fig. 6A). This result suggests that *Dys* and *Cvc* function in the same or parallel pathways. Thirdly, we tried to rescue the effect on transmitter release observed in Dys^{E6} mutants by simultaneously removing the possible target of Cv-c. The rationale for this experiment is that if Dys and Cv-c act to negatively regulate Rho GTPase signaling than removing potential Rho substrates in either mutant background would suppress their increased neurotransmitter release. Therefore, we first determined which Rho GTPase might suppress the *cv-c* synaptic phenotype. In other studies it had been shown that Rho1, Rac1, Rac2 and Cdc42 were tissue specific targets of Cv-c in the Malpighian tubuli and the epidermis and in cell free assays (Denholm et al., 2005; Sato et al., 2010). We find that removing one copy of Cdc42 in the background of *cv-c*1 restored neurotransmitter release to wild type levels (Fig. 6B). No interaction was found with rho1 or rac1 (data not shown). Interestingly, reduced levels of Cdc42 also rescue the increased QC observed in the Dys^{E6} mutant (Fig. 6B), further suggesting that Dystrophin DLP2 functions to regulate a Rho GTPase signaling pathway required for homeostasis of the *Drosophila* third instar larval NMJ.

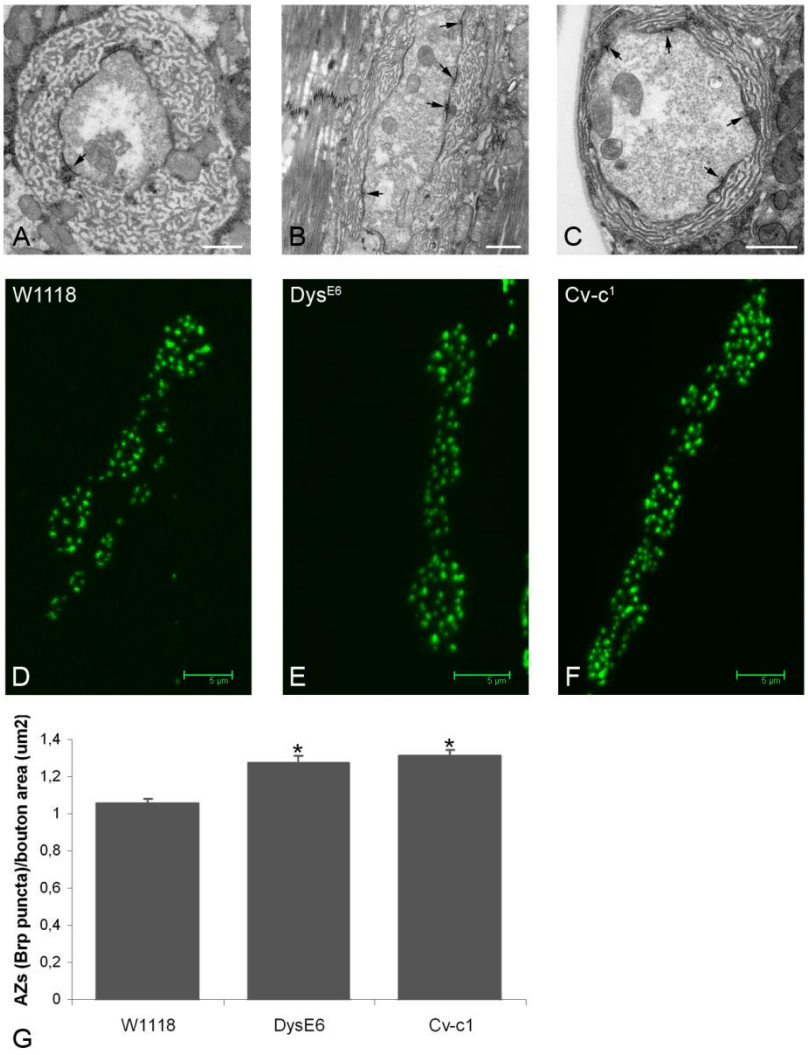

Figure 5. The number of active zones with T-bars per bouton is increased in the absence of RhoGAP *cv-c*. Using electron microscopy, no major change of the bouton morphology of NMJs of muscle 6 and 7 was observed among w^{1118} (**A**) Dys^{E6} (**B**), and *cv-c*^{1} (**C**) larvae, except for an increase in T bars, indicated by arrows. Scale bar= 1 µm. NC82 antibody stainings of w^{1118} (**D**) Dys^{E6} (**E**) and *cv-c*^{1} (**F**) larval bodywalls are shown. Scale bar = 5 µm. (**G**) Bar graph of the number of NC82 positive active zones per bouton area is shown for each genotype (N=5), showing a significant increase for Dys^{E6} (1.31±0.03; n=98) and *cv-c*^{1} (1.28±0.04; n=97) compared to the wild type control w^{1118} (1.06±0.02; n=78). *p<0.001.

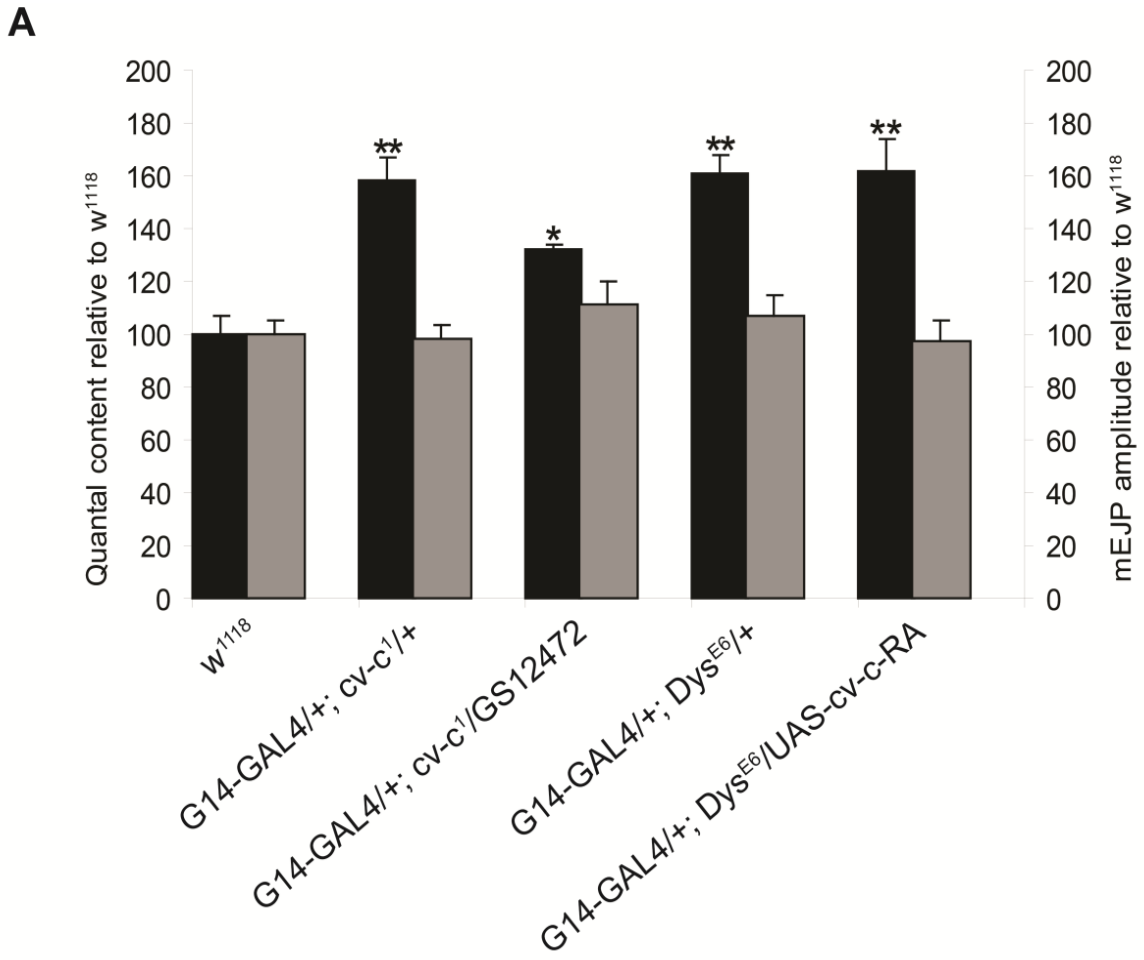

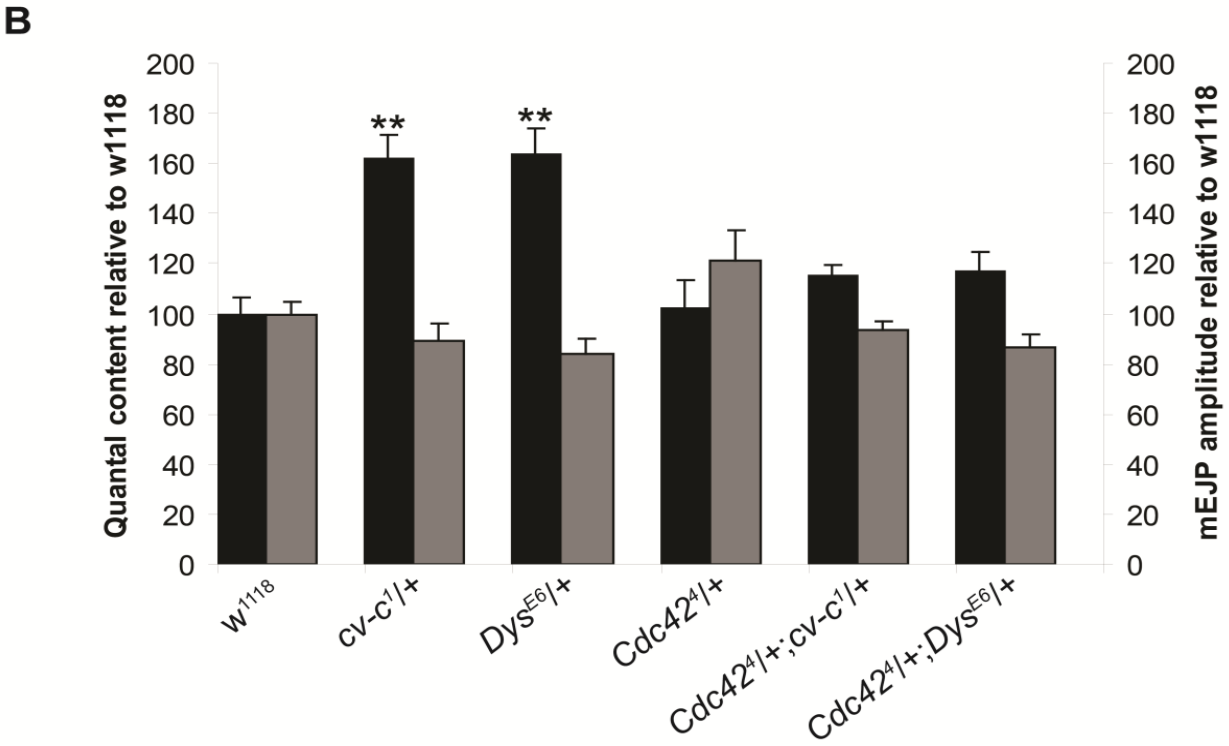

Figure 6. *Dys* interacts with a Rho GTPase signaling pathway at the larval NMJ. Bar graph representations are shown of the mean ± SEM values of the QC (left Y-axis, dark bars) and the mEJP amplitudes (right Y-axis, light bars) normalized to wild type controls recorded from w1118 third instar larvae. (A) Overexpression of RhoGAP *cv-c* in the heterozygous Dys^{E6} mutant muscle fibers does not reduce the increased QC level, while overexpression of Dys in the muscle in the heterozygous *cv-c*1 mutant partially reduces the otherwise increased QC towards wild type levels. (B) Heterozygosity for the Cdc424 mutant allele in either the heterozygous *cv-c*1 or Dys^{E6} mutant background restores QC to wild type levels. This suggests that Cdc42 is a substrate of Cv-c in a homeostatic signaling pathway operating at the NMJ and that Dystrophin genetically interacts with the Rho GTPase signaling pathway. All measured values are presented in Suppl. Table 2.

Discussion

During development, homeostatic mechanisms ensure that levels of neurotransmitter release are adjusted to compensate for the dramatic increases in the size of synaptic terminals and their targets. At the NMJ, achieving appropriate synaptic homeostatic endpoints requires retrograde signaling from the muscle to the motoneuron, a process which has been studied extensively in *Drosophila* (reviewed in Marques and Zhang, 2006). Some of these retrograde molecular pathways, such as the BMP pathway, are also involved in synaptic growth (Aberle et al., 2002; McCabe et al., 2003, Ball et al., 2010), while mutations in other genes can prevent appropriate synaptic homeostasis without visible effect on synapse size or overall morphology (Haghighi et al., 2003; Frank et al., 2006; Dickman and Davis, 2009). The challenges ahead include understanding how the latter types of

pathways regulate synapse function. We previously reported that the absence of the postsynaptic Dys DLP2 isoform results in elevated presynaptic neurotransmitter release at the *Drosophila* NMJ (van der Plas et al., 2006). Here, we made use of a wing crossvein phenotype exhibited by the Dys^{E6} DLP2 mutant to perform a genetic screen for *Dys* interacting genes whose possible functions at the NMJ could be subsequently determined. We identified the RhoGAP *cv-c* as a *Dys* mutant modifier. While this screen was in progress, other genes that interact with *Dys* during wing vein formation were reported (Christoforou et al., 2007; Kucherenko et al., 2008). *cv-c* was not found as an enhancer of *Dys* in these studies, however, the genes mutated were not identified for the majority of the EMS-induced modifiers(Kucherenko et al., 2008), leaving open the possibility that *cv-c* was among them. We determined that Cv-c is expressed postsynaptically at the NMJ and found that overall synapse morphology and postsynaptic responsiveness to neurotransmitter are unaltered in the *cv-c* mutant. Reduced expression of Cv-c results in significantly increased QC due to elevation of EJP amplitudes similar to that observed in the *Dys* mutant. Rescue and transgenic RNA interference experiments indicate that Cv-c is required postsynaptically to maintain appropriate levels of presynaptic vesicle release. Our results indicate that the elevated QC is due to an increased probability of release, associated with higher numbers of T-bars per AZ, as was previously reported for the Dys^{E6} DLP2 mutant (van der Plas et al., 2006) and for animals with decreased postsynaptic CAMKII activity (Haghighi et al., 2003). The *brp* (Kittel et al., 2006) and *unc-51* (Wairkar et al., 2009) mutant NMJs lack T-bars, display low QC and, at least for *brp*, are not in a facilitated state as determined by paired-pulse assays. Conversely, the few remaining active synaptic sites at the *rab3* mutant NMJ display elevated neurotransmitter release due to increased T-bar density (Graf et al., 2009). Together with our findings that *dys* and *cv-c* mutant NMJs are in a facilitated state and have increased numbers of T-bars, Brp+ punctae and elevated QC, these results provide further support for the hypothesis that increased numbers of T-bars correlate with increased QC and synaptic facilitation.

Insight into the interaction of *Dys* and *cv-c* came from our observation that reduced levels of the Rho GTPase Cdc42 suppress both the *cv-c* and Dys^{E6} mutant synaptic phenotype. Cv-c is a member of the RhoGAP family, which together with the RhoGEFs and RhoGDIs, controls the nucleotide state of the Rho GTPases that cycle between an inactive GDP-bound and an active GTPbound state (reviewed in Hall, 1998). RhoGAPs promote the GTP-hydrolyzing activity of the Rho GTPases, thereby increasing the level of the GDP-bound, inactive form of the GTPases. Rho signaling pathways have been shown to regulate actin cytoskeleton organization, vesicle trafficking and many other biological processes. Rho1, Rac1, Rac2 and Cdc42 have been found to be Cv-c targets both *in vivo* and in cell free enzyme assays (Denholm et al., 2005; Sato et al., 2010).

We found that removal of one copy of *Cdc42* in the $cv\text{-}c^{1}$ background completely restores wild type levels of neurotransmitter release. Heterozygosity for null alleles of *rho1* or *rac1* does not suppress the $cv\text{-}c^{1}$ synaptic phenotype, however, we cannot rule out the possibility that their expression levels are sufficiently high that halving them does not bring them below the threshold necessary to see suppression. The observation that heterozygosity for *Cdc42* essentially completely suppresses the *cv-c* phenotype indicates, however, that it is likely the principle Rho GTPase gene interacting with *cv-c* to regulate presynaptic neurotransmitter release. Moreover, reduction of *Cdc42* levels in the Dys^{E6} mutant background also suppresses the increase in neurotransmitter release, providing further evidence that Dys and Cv-c act together via Cdc42 to maintain normal synaptic function. *Cv-c* and *Dys* are both required postsynaptically to maintain wild type levels of neurotransmitter release. When we overexpressed Dys postsynaptically in the heterozygous $cv\text{-}c^{1}$ mutant, we observed a limited, but significant, decrease in QC. This apparent partial rescue might be due to the increased

recruitment of other RhoGAPS by overexpressed Dys. Postsynaptic overexpression of *cv-c* did not rescue the heterozygous Dys^{E6} mutant phenotype possibly due to the failure of Cv-c to localize properly in the absence of Dys. While it remains unclear how Cv-c and Dys interact, we hypothesize that decreased Dys levels result in a reduction of the activity of Cv-c leading to increased activity of Cdc42. The genetic interaction of *cv-c* and *Cdc42* may indicate that Cdc42 is a direct target of Cv-c. However, it is also possible that the two genes act in either parallel pathways or in a single trans-synaptic pathway in which other RhoGAPs act upon presynaptic Cdc42. The former possibility is consistent with proposed models for the regulation of synaptic homeostasis in which multiple feedback mechanisms are predicted to act simultaneously in parallel pathways (Davis, 2006). With respect to the possibility of a single trans-synaptic pathway, *Cdc42* has been shown to interact genetically with the presynaptic RhoGEF gene, *ephexin* (*exn*) whose protein product functions downstream of the Ephrin receptor to regulate the Cacophony (Cac) calcium channel (Frank et al., 2009). This pathway mediates rapid NMJ homeostasis and is also likely involved in slower long-term homeostatic responses as *Cac* was previously shown to be required for the compensatory increases in QC observed in the GluRIIA glutamate receptor mutant (Frank et al., 2006). Although *exn* (Frank et al., 2009) and *cv-c* (this work) were shown to act pre- and postsynaptically, respectively, neither study formally demonstrated where *Cdc42* is required for homeostasis. Thus, it remains possible that Cdc42 plays roles in separate pre- and postsynaptic homeostatic pathways or in a single trans-synaptic pathway at one or both sides of the synapse.

The interactions of *dys* and Rho GTPase signaling during synaptic homeostasis could converge on, among other postsynaptic processes, cytoskeletal remodeling, clustering of neurotransmitter receptors or Ca^{2+} handling. Synaptic actin networks play dynamic roles in modulating pre- and postsynaptic synaptic function (Cingolani and Goda, 2008). The postsynaptically localized DLP2 isoform bears the conserved Dystrophin aminoterminal actin-binding domain. However, while the importance of this domain for Dystrophin's sarcolemmal interactions has been established (Judge et al, 2006), its role at the synapse has not been reported. Further cytoskeletal interactions of Dystrophin at the NMJ were revealed by the analysis of Ankyrin-deficient mice (Ayalon et al, 2008). Ankyrin stabilizes membrane-associated microtubule networks and is required for the localization of Dystrophin and other DGC proteins to the NMJ. There have been several reports of Rho pathway involvements in postsynaptic receptor clustering. The *Drosophila* RhoGEF, RtGEF (dPix), regulates the postsynaptic localization of GluRIIA through the Cdc42 effector kinase dPak (Parnas et al., 2001). Absence of dPix also compromises retrograde signaling, as reflected by reduced mEJPs and EJPs amplitudes (Parnas et al., 2001). Similarly, the extracellular Dystroglycan-binding proteins, Laminin and Agrin, both signal through Rho GTPase-dependent pathways to initiate AChR clustering (Weston et al., 2007). Finally, there is evidence for a RhoA-dependent postsynaptic role of *ephexin-1* in regulation of clustering of acetylcholine neurotransmitter receptors at the murine NMJ (Shi et al., 2010). However, a role for *Dys* and/or *cv-c* in postsynaptic receptor clustering at the NMJ is unlikely since we observed no apparent changes in the number or location of the glutamate receptors in their respective mutant animals.

Lastly, changes in Ca^{2+} flux in response to the Dys/Cv-c/Cdc42 pathway may underlie the aberrant homeostatic endpoints observed at the *Dys* and *cv-c* mutant NMJs. Mammalian Dystrophin-deficient muscle fibers have extensively studied deficits in Ca^{2+} handling (reviewed in Hopf et al., 2007). Interestingly, postsynaptic inhibition of Calcium/calmodulin-dependent kinase II (CAMKII) results in increased QC at the *Drosophila* NMJ (Haghighi et al., 2003). While Dystrophin and CAMKII are known to interact physically via evolutionarily conserved motifs (reviewed in Michalak et al., 1996), they have yet to be functionally linked at the NMJ.

At present, therefore, there are a number of potential targets of the Rho GTPase pathway which is disturbed in the Dys^{E6} mutant. Identifying the targets of the Cvc/Cdc42 pathway at the NMJ will increase our understanding of Dystrophin's role at the synapse and likely lead to the identification of more general aspects of the pathways contributing to synaptic homeostasis.

Acknowledgements: We thank Renée Bakker for help with the initial experiments, the Bloomington *Drosophila* Stock Center, R. Ray and M. O'Connor for fly stocks, and J. Plomp and R. Ray for their comments on the manuscript. This work was funded by the 'Nederlandse Organisatie voor Wetenschappelijk Onderzoek', 'N.W.O.'

References

Aberle H, Haghighi AP, Fetter RD, McCabe BD, Magalhaes TR, Goodman CS (2002) wishful thinking encodes a BMP type II receptor that regulates synaptic growth in *Drosophila*. Neuron 33:545-558.

Anderson JL, Head SI, Rae C, Morley JW (2002) Brain function in Duchenne muscular dystrophy. Brain 125:4-13.

Billuart P, Winter CG, Maresh A, Zhao X, Luo L (2001) Regulating axon branch stability: the role of p190 RhoGAP in repressing a retraction signaling pathway. Cell 107:195-207.

Billuart P, Bienvenu T, Ronce N, des PV, Vinet MC, Zemni R, Carrie A, Beldjord C, Kahn A, Moraine C, Chelly J (1998) Oligophrenin 1 encodes a rho-GAP protein involved in X-linked mental retardation. PatholBiol(Paris) 46:678.

Boyd IA, Martin AR (1956) The End-Plate Potential in Mammalian Muscle. Journal of Physiology-London 132:74-91.

Brand AH, Perrimon N (1993) Targeted gene expression as a means of altering cell fates and generating dominant phenotypes. Development 118:401-415.

Chockalingam PS, Cholera R, Oak SA, Zheng Y, Jarrett HW, Thomason DB (2002) Dystrophin-glycoprotein complex and Ras and Rho GTPase signaling are altered in muscle atrophy. AmJ Physiol Cell Physiol 283:C500-C511.

Christoforou CP, Greer CE, Challoner BR, Charizanos D, Ray RP (2007) The detached locus encodes *Drosophila* Dystrophin, which acts with other components of the Dystrophin Associated Protein Complex to influence intercellular signalling in developing wing veins. DevBiol.

Crozatier M, Glise B, Vincent A (2004) Patterns in evolution: veins of the *Drosophila* wing. Trends Genet 20:498-505.

Davis GW, Bezprozvanny I (2001) Maintaining the stability of neural function: a homeostatic hypothesis. AnnuRevPhysiol 63:847-869.

De Celis JF (2003) Pattern formation in the *Drosophila* wing: The development of the veins. Bioessays 25:443-451.

Denholm B, Brown S, Ray RP, Ruiz-Gomez M, Skaer H, Hombria JC-G (2005) crossveinless-c is a RhoGAP required for actin reorganisation during morphogenesis. Development 132:2389-2400.

DiAntonio A, Petersen SA, Heckmann M, Goodman CS (1999) Glutamate receptor expression regulates quantal size and quantal content at the *Drosophila* neuromuscular junction. Journal of Neuroscience 19:3023-3032.

Dickman DK, Davis GW (2009) The Schizophrenia Susceptibility Gene dysbindin Controls Synaptic Homeostasis. Science 326:1127-1130.

Featherstone DE, Rushton E, Rohrbough J, Liebl F, Karr J, Sheng Q, Rodesch CK, Broadie K (2005) An essential *Drosophila* glutamate receptor subunit that functions in both central neuropil and neuromuscular junction. Journal of Neuroscience 25:3199-3208.

Fradkin LG, Baines RA, van der Plas MC, Noordermeer JN (2008) The dystrophin Dp186 isoform regulates neurotransmitter release at a central synapse in *Drosophila*. J Neurosci 28:5105-5114.

Frank CA, Pielage J, Davis GW (2009) A presynaptic homeostatic signaling system composed of the Eph receptor, ephexin, Cdc42, and CaV2.1 calcium channels. Neuron 61:556-569.

Frank CA, Kennedy MJ, Goold C, Marek KW, Davis G (2006) Mechanisms Underlying the Rapid Induction and Sustained Expression of Synaptic Homeostasis. Neuron 52:663-677.

Gauthier-Rouviere C, Bonet-Kerrache A (2009) RhoA leads to up-regulation and relocalization of utrophin in muscle fibers. BiochemBiophysResCommun 384:322-328.

Govek EE, Newey SE, Van AL (2005) The role of the Rho GTPases in neuronal development. Genes Dev 19:1-49.

Haghighi AP, McCabe BD, Fetter RD, Palmer JE, Hom S, Goodman CS (2003) Retrograde control of synaptic transmission by postsynaptic CaMKII at the *Drosophila* neuromuscular junction. Neuron 39:255-267.

Hall A (1998) Rho GTPases and the actin cytoskeleton. Science 279:509-514.

Hoffman EP, Brown RH, Kunkel LM (1987) Dystrophin: The protein product of the duchenne muscular dystrophy locus. Cell 51:919-928.

Kittel RJ, Hallermann S, Thomsen S, Wichmann C, Sigrist SJ, Heckmann M (2006) Active zone assembly and synaptic release. Biochemical Society Transactions 34:939-941.

Koenig M, Hoffman EP, Bertelson CJ, Monaco AP, Feener C, Kunkel LM (1987) Complete cloning of the Duchenne muscular dystrophy (DMD) cDNA and preliminary genomic organization of the DMD gene in normal and affected individuals. Cell 50:509-517.

Kucherenko MM, Pantoja M, Yatsenko AS, Shcherbata HR, Fischer KA, Maksymiv DV, Chernyk YI, Ruohola-Baker H (2008) Genetic modifier screens reveal new components that interact with the *Drosophila* dystroglycan-dystrophin complex. PLoSOne 3:e2418.

Luo L, Liao YJ, Jan LY, Jan YN (1994) Distinct morphogenetic functions of similar small GTPases: *Drosophila* Drac1 is involved in axonal outgrowth and myoblast fusion. Genes Dev 8:1787-1802.

Malacombe M, Ceridono M, Calco V, Chasserot-Golaz S, McPherson PS, Bader MF, Gasman S (2006) Intersectin-1L nucleotide exchange factor regulates secretory granule exocytosis by activating Cdc42. EMBO J 25:3494-3503.

Marques G, Zhang B (2006) Retrograde signaling that regulates synaptic development and function at the *Drosophila* neuromuscular junction.

McCabe BD, Marques G, Haghighi AP, Fetter RD, Crotty ML, Haerry TE, Goodman CS, O'Connor MB (2003) The BMP homolog Gbb provides a retrograde signal that regulates synaptic growth at the *Drosophila* neuromuscular junction. Neuron 39:241-254.

Nakano-Kobayashi A, Kasri NN, Newey SE, Van Aelst L (2009) The Rho-linked mental retardation protein OPHN1 controls synaptic vesicle endocytosis via endophilin A1. Curr Biol 19:1133-1139.

Newey SE, Velamoor V, Govek EE, Van AL (2005) Rho GTPases, dendritic structure, and mental retardation. J Neurobiol 64:58-74.

Ng J, Luo L (2004) Rho GTPases regulate axon growth through convergent and divergent signaling pathways. Neuron 44:779-793.

Parnas D, Haghighi AP, Fetter RD, Kim SW, Goodman CS (2001) Regulation of Postsynaptic Structure and Protein Localization by the Rho-Type Guanine Nucleotide Exchange Factor dPix. Neuron 32:415-424.

Petersen SA, Fetter RD, Noordermeer JN, Goodman CS, DiAntonio A (1997) Genetic analysis of glutamate receptors in *Drosophila* reveals a retrograde signal regulating presynaptic transmitter release. Neuron 19:1237-1248.

Pilgram GS, Potikanond S, Baines RA, Fradkin LG, Noordermeer JN (2010) The roles of the dystrophin-associated glycoprotein complex at the synapse. MolNeurobiol 41:1-21.

Plomp JJ, van Kempen GT, Molenaar PC (1992) Adaptation of quantal content to decreased postsynaptic sensitivity at single endplates in alpha-bungarotoxin-treated rats. J Physiol 458:487-499.

Ramakers GJA (2002) Rho proteins, mental retardation and the cellular basis of cognition. Trends in Neurosciences 25:191-199.

Rando TA (2001) The dystrophin-glycoprotein complex, cellular signaling, and the regulation of cell survival in the muscular dystrophies. Muscle Nerve 24:1575-1594.

Rapaport D, Passos-Bueno MR, Brandao L, Love D, Vainzof M, Zatz M (1991) Apparent association of mental retardation and specific patterns of deletions screened with probes cf56a and cf23a in Duchenne muscular dystrophy. AmJ MedGenet 39:437-441.

Roberts RG, Bobrow M (1998) Dystrophins in vertebrates and invertebrates. Human Molecular Genetics 7:589-595.

Rohrbough J, Pinto S, Mihalek RM, Tully T, Broadie K (1999) latheo, a *Drosophila* gene involved in learning, regulates functional synaptic plasticity. Neuron 23:55-70.

Sandstrom DJ (2004) Isoflurane depresses glutamate release by reducing neuronal excitability at the *Drosophila* neuromuscular junction. J Physiol 558:489-502.

Schuster CM, Ultsch A, Schloss P, Cox JA, Schmitt B, Betz H (1991) Molecular cloning of an invertebrate glutamate receptor subunit expressed in *Drosophila* muscle. Science 254:112-114.

Shcherbata HR, Yatsenko AS, Patterson L, Sood VD, Nudel U, Yaffe D, Baker D, Ruohola-Baker H (2007) Dissecting muscle and neuronal disorders in a *Drosophila* model of muscular dystrophy. EMBO J 26:481-493.

Shi L, Butt B, Ip FC, Dai Y, Jiang L, Yung WH, Greenberg ME, Fu AK, Ip NY (2010) Ephexin1 is required for structural maturation and neurotransmission at the neuromuscular junction. Neuron 65:204-216.

Sigrist SJ, Thiel PR, Reiff DF, Schuster CM (2002) The postsynaptic glutamate receptor subunit DGluR-IIA mediates long-term plasticity in *Drosophila*. Journal of Neuroscience 22:7362-7372.

Stewart BA, Atwood HL, Renger JJ, Wang J, Wu CF (1994) Improved stability of *Drosophila* larval neuromuscular preparations in haemolymph-like physiological solutions. J Comp Physiol [A] 175:179-191.

Taghli-Lamallem O, Akasaka T, Hogg G, Nudel U, Yaffe D, Chamberlain JS, Ocorr K, Bodmer R (2008) Dystrophin deficiency in *Drosophila* reduces lifespan and causes a dilated cardiomyopathy phenotype. Aging Cell 7:237-249.

Tautz D, Pfeifle C (1989) A non-radioactive in situ hybridization method for the localization of specific RNAs in *Drosophila* embryos reveals translational control of the segmentation gene hunchback. Chromosoma 98:81-85.

Toba G, Ohsako T, Miyata N, Ohtsuka T, Seong KH, Aigaki T (1999) The gene search system. A method for efficient detection and rapid molecular identification of genes in *Drosophila* melanogaster. Genetics 151:725-737.

Turrigiano GG, Nelson SB (2004) Homeostatic plasticity in the developing nervous system. NatRevNeurosci 5:97-107.

van der Plas MC, Pilgram GS, Plomp JJ, de JA, Fradkin LG, Noordermeer JN (2006) Dystrophin is required for appropriate retrograde control of neurotransmitter release at the *Drosophila* neuromuscular junction. J Neurosci 26:333-344.

van der Plas MC, Pilgram GSK, de Jong AWM, Bansraj MRKS, Fradkin LG, Noordermeer JN (2007) *Drosophila* Dystrophin is required for integrity of the musculature. Mechanisms of Development 124:617-630.

Van Vactor D, Sink H, Fambrough D, Tsoo R, Goodman CS (1993) Genes that control neuromuscular specificity in *Drosophila*. Cell 73:1137-1153.

Wagh DA, Rasse TM, Asan E, Hofbauer A, Schwenkert I, Durrbeck H, Buchner S, Dabauvalle MC, Schmidt M, Qin G, Wichmann C, Kittel R, Sigrist SJ, Buchner E (2006) Bruchpilot, a protein with homology to ELKS/CAST, is required for structural integrity and function of synaptic active zones in *Drosophila*. Neuron 49:833-844.

Waite A, Tinsley CL, Locke M, Blake DJ (2009) The neurobiology of the dystrophin-associated glycoprotein complex. AnnMed 41:344-359.

Weston CA, Teressa G, Weeks BS, Prives J (2007) Agrin and laminin induce acetylcholine receptor clustering by convergent, Rho GTPase-dependent signaling pathways. Journal of Cell Science 120:868-875.

Zucker RS, Regehr WG (2002) Short-term Synaptic Plasticity. Annual Review of Physiology 64:355-405.

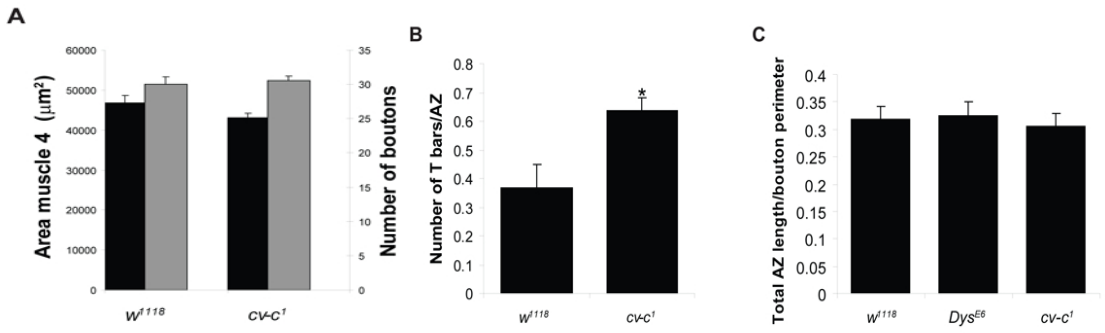

Supplemental Figure 1. Muscle size and bouton number are not changed in *cv-c* mutants. Larval body walls were stained with anti-FasII to label the boutons of the motoneurons. Both muscle area (black bar and left y-axis) and the number of boutons (gray bar and right y-axis) do not significantly differ between the wild type w^{1118} control and $cv\text{-}c^{1}$ mutant.

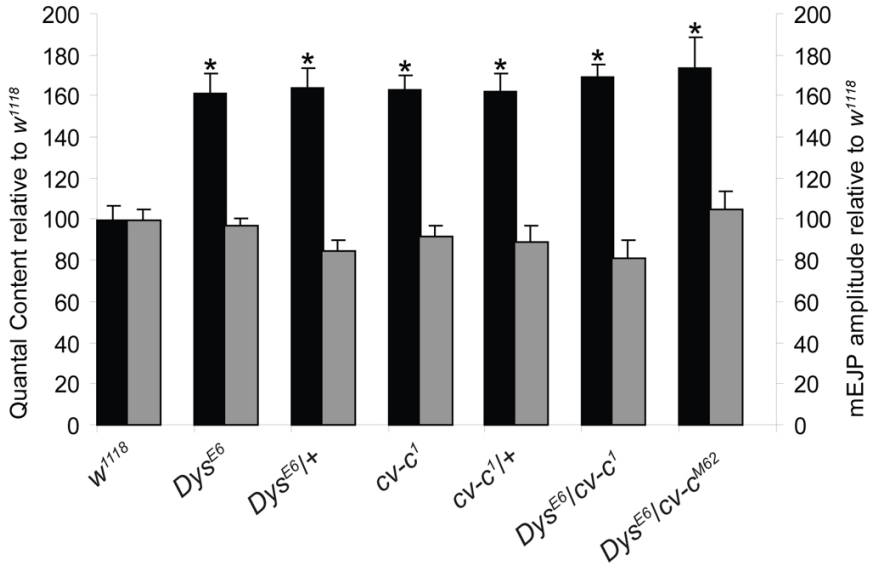

Supplemental Figure 2. Analysis of the physiology of *Dys*/*cv-c* transheterozygotes. Bar graph representations are shown of the mean ± SEM of the QC (left Y-axis, black bars) and the mEJP amplitudes (right Y-axis, gray bars) normalized to wild type controls recorded from w^{1118} third instar larvae (n=24), Dys^{E6} (n=15), Dys^{E6}/+ (n=9), $cv\text{-}c^{1}$ (n=16), $cv\text{-}c^{1}$/+ (n=9), $Dys^{E6}/cv\text{-}c^{1}$ (n=5), and $Dys^{E6}/\ cv\text{-}c^{M62}$ (n=5). [**QCs**: 39.8±2.6 in w^{1118}, 64.1±3.8 in Dys^{E6}, 65.2±3.9 in Dys^{E6}/+, 64.9±2.6 in $cv\text{-}c^{1}$, 64.4±3.6 in $cv\text{-}c^{1}$/+, 67.1±2.6 in $Dys^{E6}/cv\text{-}c^{1}$, 69.2±5.7 in $Dys^{E6}/cv\text{-}c^{M62}$ larvae; **mEJPs**: 0.71±0.04 mV in w^{1118},0.69±0.03 mV in Dys^{E6},0.60±0.04 mV in Dys^{E6}/+, 0.65±0.04 mV in $cv\text{-}c^{1}$, 0.63±0.05 mV in $cv\text{-}c^{1}$/+, 0.74±0.7 mV in $Dys^{E6}/cv\text{-}c^{M62}$ larvae].

Supplemental Table 1. Alphabetical ordering according to genotype of all averaged electrophysiological data, including the frequencies of mEJPs (fmEJPs), mEJPs, EJPs and quantal content (QC)

Genotype		fmEJP	mEJP	EJP	QC
cv-c^{C524}/+	Mean	2.54	0.75	34.89	67.42
	Std. Error of Mean	0.29	0.05	0.62	3.83
	N	6	6	6	6
cdc42^{4}/+	Mean	2.79	0.86	25.71	40.52
	Std. Error of Mean	0.55	0.08	1.25	4.63
	N	6	6	6	6
cdc42^{4}/*cv-c*^{1}	Mean	2.34	0.66	23.78	45.84
	Std. Error of Mean	0.50	0.03	0.91	1.70
	N	7	7	7	7
cdc42^{4}/*Dys*^{E6}	Mean	2.71	0.62	22.82	46.55
	Std. Error of Mean	0.29	0.04	1.46	2.98
	N	11	11	11	11
cv-c^{1}/*cv-c*^{C524}	Mean	3.27	0.66	33.78	71.40
	Std. Error of Mean	0.62	0.02	0.98	5.15
	N	6	6	6	6
cv-c^{1}/*cv-c*^{M62}	Mean	3.27	0.69	34.61	71.79
	Std. Error of Mean	0.68	0.03	2.08	5.70
	N	6	6	6	6
cv-c^{M62}/+	Mean	3.26	0.74	32.60	60.38
	Std. Error of Mean	0.36	0.05	1.49	2.61
	N	7	7	7	7
cv-c^{M62}/*Dys*^{E6}	Mean	4.04	0.74	35.10	69.16
	Std. Error of Mean	0.26	0.07	1.67	5.69
	N	5	5	5	5
cv-c^{1}	Mean	3.08	0.65	30.44	64.89
	Std. Error of Mean	0.41	0.04	1.07	2.58
	N	20	20	20	20
cv-c^{1}/+	Mean	2.63	0.63	29.62	64.43
	Std. Error of Mean	0.33	0.05	1.65	3.61
	N	9	9	9	9
Dys^{E6}	Mean	4.50	0.70	32.29	64.77
	Std. Error of Mean	0.47	0.03	1.24	3.47
	N	12	12	12	12
Dys^{E6}/*cv-c*^{1}	Mean	3.66	0.58	28.97	67.08
	Std. Error of Mean	0.81	0.06	2.06	2.62
	N	5	5	5	5
Dys^{E6}/+	Mean	2.60	0.60	28.66	65.18
	Std. Error of Mean	0.41	0.04	1.31	3.89
	N	9	9	9	9
G14-Gal4/+	Mean	1.65	0.80	25.42	40.61
	Std. Error of Mean	0.25	0.06	1.96	2.02
	N	5	5	5	5

G14-Gal4/+;*cv-c*^{1}/+	Mean	1.67	0.70	31.95	62.89
	Std. Error of Mean	0.15	0.04	0.47	3.50
	N	6	6	6	6
G14-Gal4/+;*cv-c*^{1}/GS12472	Mean	2.49	0.79	30.38	52.42
	Std. Error of Mean	0.50	0.06	1.80	0.69
	N	5	5	5	5
G14-Gal4/+;*cv-c*^{1}/UAS-*cv-c*-RA	Mean	1.50	0.74	26.79	47.85
	Std. Error of Mean	0.26	0.08	2.04	2.81
	N	6	6	6	6
G14-Gal4/+;*Dys*^{E6}/+	Mean	2.76	0.76	34.29	63.87
	Std. Error of Mean	0.43	0.06	1.09	2.80
	N	4	4	4	4
G14-Gal4/+;*Dys*^{E6}/UAS-*cv-c*-RA	Mean	2.36	0.69	32.22	64.34
	Std. Error of Mean	0.27	0.05	1.84	4.72
	N	5	5	5	5
G14/RNAi-*cv-c*	Mean	1.90	0.65	32.40	68.38
	Std. Error of Mean	0.19	0.02	1.46	3.25
	N	7	7	7	7
OK6-Gal4/+;*Cv-c*^{1}/+	Mean	2.26	0.63	31.91	70.08
	Std. Error of Mean	0.28	0.04	0.99	6.37
	N	6	6	6	6
OK6-Gal4/+	Mean	3.50	0.83	27.25	43.51
	Std. Error of Mean	0.55	0.02	1.16	2.65
	N	15	15	15	15
OK6-Gal4/+;*cv-c*^{1}/UAS-*cv-c*-RA	Mean	2.28	0.68	32.17	65.17
	Std. Error of Mean	0.32	0.03	0.77	3.48
	N	6	6	6	6
OK6-Gal4/RNAi-*cv-c*	Mean	3.21	0.83	31.01	52.21
	Std. Error of Mean	0.24	0.05	1.51	4.52
	N	9	9	9	9
w^{1118}	Mean	2.34	0.71	21.62	39.75
	Std. Error of Mean	0.28	0.04	1.12	2.60
	N	24	24	24	24